iScience

CellPress
OPEN ACCESS

Article

# Combined influence of soil moisture and atmospheric humidity on land surface temperature under different climatic background

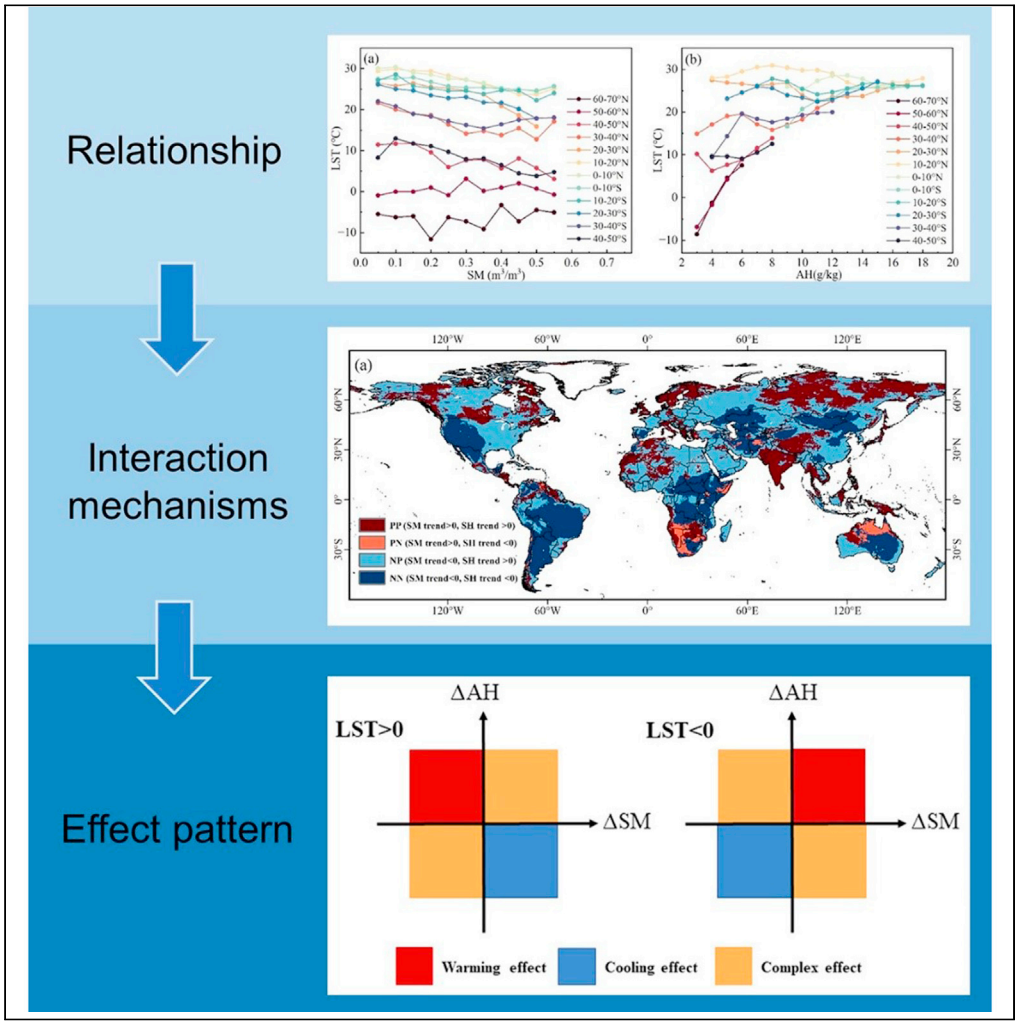


Kang Jiang, Zhihua Pan, Feifei Pan, ..., Jingyu Men, Xiaoqin Lv, Zhiqiang Dong

panzhihua@cau.edu.cn

## Highlights

SM played essential and different roles under the different LST backgrounds

The AH always displayed a greenhouse effect on the LST

Net radiation, SM, and AH could explain 92% of the global LST change

Jiang et al., iScience 26, 106837
June 16, 2023 
https://doi.org/10.1016/j.isci.2023.106837

iScience

CellPress
OPEN ACCESS

Article

# Combined influence of soil moisture and atmospheric humidity on land surface temperature under different climatic background

Kang Jiang,[1,2] Zhihua Pan,[1,2,10,*] Feifei Pan,[3] Adriaan J. Teuling,[4] Guolin Han,[5] Pingli An,[6,7] Xiao Chen,[1,2] Jialin Wang,[1,6] Yu Song,[1,2] Lu Cheng,[8] Ziyuan Zhang,[1,2] Na Huang,[1,2] Shangqian Ma,[1,2] Riping Gao,[1,2] Zhenzhen Zhang,[1,2] Jingyu Men,[1,2] Xiaoqin Lv,[1,2] and Zhiqiang Dong[9]

## SUMMARY

**Soil moisture (SM) and atmospheric humidity (AH) are crucial climatic variables that significantly affect the climate system. However, the combined influencing mechanisms of SM and AH on the land surface temperature (LST) under global warming are still unclear. Here, we systematically analyzed the interrelationships among annual mean values of SM, AH, and LST using ERA5-Land reanalysis data and revealed the role of SM and AH on the spatiotemporal variations of LST through mechanism analysis and regression methods. The results showed that net radiation, SM, and AH could well model the long-term variability of LST well and explain 92% of the variability. Moreover, SM played an essential and different role under the different LST backgrounds. The AH always displayed a greenhouse effect on the LST. This study provides essential insights into the global climate change mechanism from the surface hydrothermal processes perspective.**

## INTRODUCTION

Land surface temperature (LST) is one of the most important and commonly used temperature monitoring indicators because it is essential for land surface energy and water balance processes.[1] Also, LST is an important fundamental indicator for global climate change monitoring. According to the IPCC Sixth Assessment Report, the global surface temperature was 1.09°C higher in 2011–2020 than in 1850–1900.[2] The increase in temperature has important implications on events such as ecological community stability,[3,4] surface evaporation,[5] and land cover change.[6–8] Therefore, the reasons for LST variations have received much more attention.

Currently, a large number of scholars have studied the causes of LST changes from many different perspectives. For example, some researchers analyzed them from the perspective of land use and land cover, believing that climatic effects due to land cover changes are particularly important for LST.[9–12] Some research focused on the trends and differences in LST changes between urban and suburban areas,[13] arguing that surface hydrothermal changes due to urbanization are responsible for LST changes. And some other researchers analyzed the relationship between LST and other single influence factor such as soil moisture (SM),[14] atmospheric humidity (AH),[15] and precipitation.[16] Their results showed that all these factors have important influence on the LST variation and there is interaction between them. However, a closer look can reveal that SM, AH, and net radiation (NR) are considered to be the key factors affecting LST. Water, including SM and AH, is the most crucial regulator of the earth's climate due to its large heat capacity and unique three-phase conversion attribute. It is a prerequisite for maintaining equilibrium in marine and terrestrial ecosystems.[16–19] NR is the source of energy and is the determining factor of the LST variation in one year. All other elements are directly or indirectly related to these three factors and thus influence the hydrothermal processes at the land surface.

Regarding the effect of water on LST, previous studies mainly focused on the effect of SM on LST because the feedback from SM is more direct.[20] They found that the interaction between SM and LST can significantly affect near-surface climate and has been shown to be an important cause of events such as heat waves[21–23] and droughts.[24,25] There is a positive feedback effect between SM and LST, the decreased

[1]College of Resources and Environmental Sciences, China Agricultural University, Beijing, China

[2]CMA-CAU Jointly Laboratory of Agriculture Addressing Climate Change, Beijing, China

[3]Department of Geography and the Environment, University of North Texas, Denton, TX, USA

[4]Hydrology and Quantitative Water Management Group, Wageningen University & Research, Wageningen, Netherlands

[5]China Meteorological Administration Training Center, Beijing, China

[6]College of Land Science and Technology, China Agricultural University, Beijing, China

[7]Key Laboratory of Land Quality, Ministry of Land and Resources, Beijing, China

[8]National Meteorological Center, Beijing, China

[9]Shandong Provincial Climate Center, Jinan, China

[10]Lead contact

*Correspondence: panzhihua@cau.edu.cn

https://doi.org/10.1016/j.isci.2023.106837

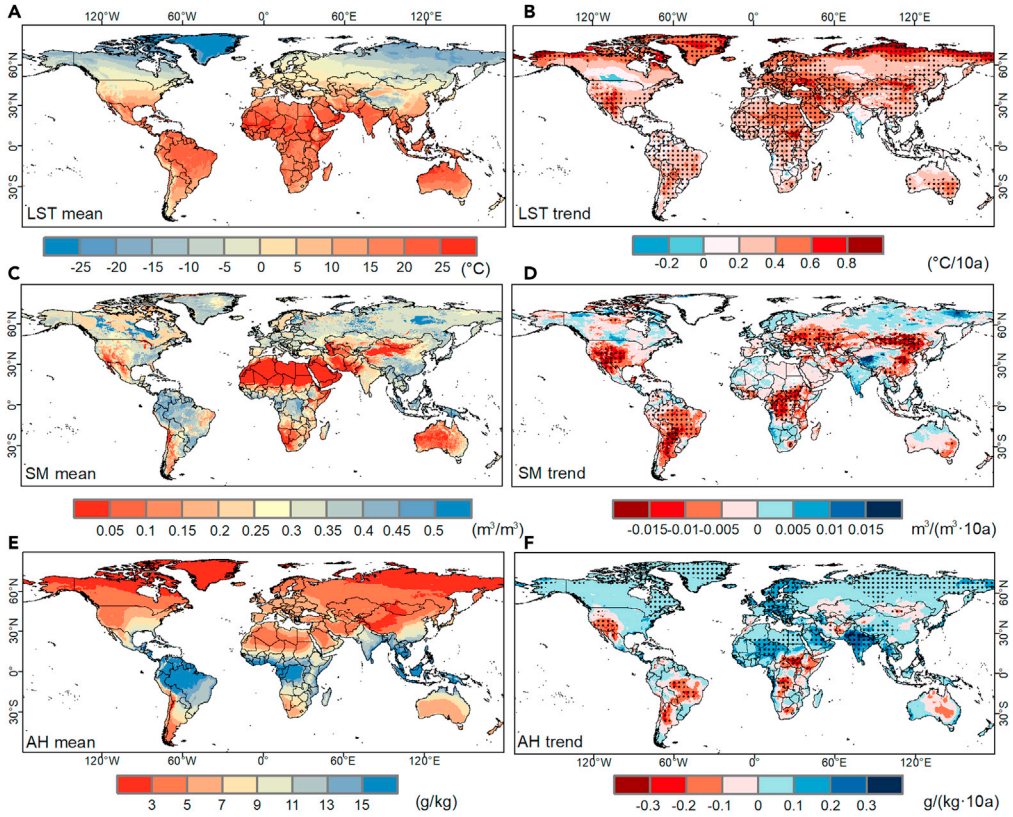


**Figure 1. Spatial and temporal variations of land surface temperature (LST)**

(A and B) Soil moisture (SM) (C and D) and atmospheric humidity (AH) (E and F). The dotted areas are temporal trend passing the significance test of $p < 0.01$.

SM will lead to an increase in land surface sensible heat flux and, thus, a rise in LST, and the increased LST further accelerates land surface evaporation, leading to lower SM.[26] More water enters into the atmosphere in a warming world and leads to the increase of radiative feedback. The contribution of AH to regional and even global temperature increases receives much attention.[27] Research showed that the temperature response to AH differed in latitude and timescale.[28] NR is the difference between the energy input and output of the land surface. The incident solar radiation generally varies less interannually. In contrast, land surface longwave radiation and atmospheric counter radiation fluctuate more due to changes in the property of the land surface and atmospheric humidity, etc.[29] Therefore, NR is also indirectly influenced by SM and AH. We can find that SM and AH have a fundamental influence on the LST. However, studies on explaining variations of annual LST using both SM and AH are limited by observations, and the complex feedbacks and quantitative analysis have yet to be well revealed.

Observations have shown that human activities such as the over-withdrawal of groundwater,[30–32] urban expansion,[33] deforestations,[34] and overgrazing[35] have made significant impacts on the surface hydrological cycle in recent decades. According to the study, about 48% of the global vegetated area exhibited a drying pattern over the past 40 years[36] The specific humidity of the global land increased by $0.08 \pm 0.04$ g/kg per decade from 1979 to 2016.[37] With the alteration of the water cycle, there must be some impact on the local, regional, and even global climate. The IPCC Sixth Assessment Report pointed out that the biophysical effects of land use change since 1750 were mainly in the form of increased surface albedo and reduced turbulent heat fluxes, which may lead to a net global cooling of about 0.1°C.[2] This result did not take into account the feedback effects of SM and AH changes. Considering human activity has affected more than 70% of the Earth's ice-free surface, an in-depth investigation of the extent to which changes in the hydrological cycle affect LST is of great scientific significance in answering the causes of global warming. The urgent scientific questions that need to be answered are what has happened to global SM and AH, and what is the combined influencing mechanism of SM and AH on LST under global warming in recent decades.

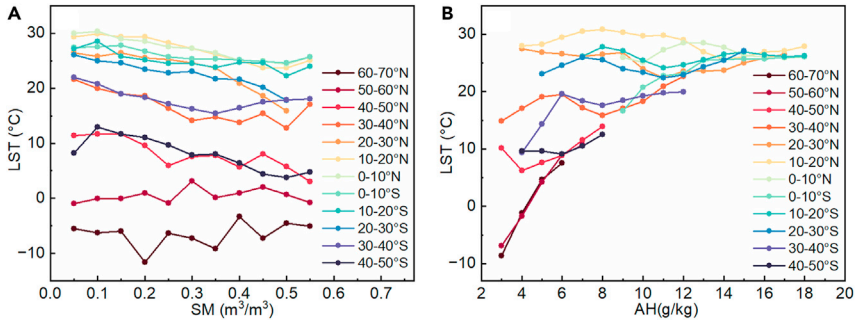


**Figure 2. Variations of land surface temperature (LST) for different**

(A) Soil moisture (SM) and (B) atmospheric humidity (AH) gradients in different latitude. Areas with altitudes above 1500 m were excluded from the analysis due to the altitude effect.

Now, global-scale studies have become possible with the rapid development of global observational techniques and model simulations.[38,39] Here, based on the principle of energy balance and ERA5-Land reanalysis data with high spatial resolution, this study explored the influence of both SM and AH on LST in different climate backgrounds using statistical analysis, and the combined influencing mechanism of SM and AH on LST under different climatic backgrounds was disclosed.

## RESULTS

### Spatial and temporal variation of LST, SM, and AH during 1981–2020

The global multi-year mean LST generally decreased with latitude (Figure 1A), with the lowest annual mean LST in Greenland below −25°C. In comparison, the LST in some parts of the equatorial region exceeded 25°C, and the annual mean LST was higher in the Sahara and the Arabian region. The LST in the Qinghai-Tibet Plateau was significantly lower than in the surrounding areas due to its high altitude. 70.7% of the global land exhibited a significant ($p < 0.01$) increasing trend in LST (Figure 1B), among which the areas with evident increase (>0.8°C/10a) were mainly located in the high latitudes of the northern hemisphere, the Mediterranean coast, southwestern North America, north-central Africa, and central-eastern Asia.

20.4% of the global land experienced a significant ($p < 0.01$) decreasing trend in SM (Figure 1D), mainly in southern North America, most of South America, central Africa, western Asia, and the Middle East. While SM in the western Tibetan Plateau, India, northeastern Asia, and central and northern North America displayed an upward trend, and the upward trend in some regions was above 0.01 $m^3/(m^3 \cdot 10a)$.

The spatial distribution of near-surface AH was similar to that of LST and generally decreased with latitude (Figure 1E). The global multi-year average AH was 6.52 g/kg. The temporal variation of near-surface AH was similar to SM (Figure 1F). The areas with significant decrease were mainly distributed in western North America, most of South America, central and southern Africa, and central and northern Australia. In contrast, the increasing trend of AH exceeded 0.2 g/(kg·10a) in regions such as India, northern Europe, and central Africa.

### Interrelationship of LST with SM and AH

The variation characteristics of LST with SM and AH in different latitudes were analyzed to investigate the relationship between LST and SM and AH (Figure 2). The LST mainly exhibited a negative relationship with SM. However, there were also some different relationships between them, i.e., decreased in the low latitude and increased in the high latitude (Figure 2A). In addition, the LST tended to decrease first and then increase with SM in some middle- and high-latitude areas (i.e., 60–70°N, 30–40°N). The LST displayed an overall increasing trend with AH (Figure 2B). The LST showed a prominent increment with AH when the AH was below 8 g/kg. While in the areas where AH was above 8 g/kg, the LST did not change much with AH.

Figure 2A showed that the different temperature backgrounds might be the essential reason for the opposite temperature trends with SM. Therefore, the impact of SM on LST under different LST background (above and below 0°C) was further analyzed (Figure 3). It was found that the areas with low SM had a

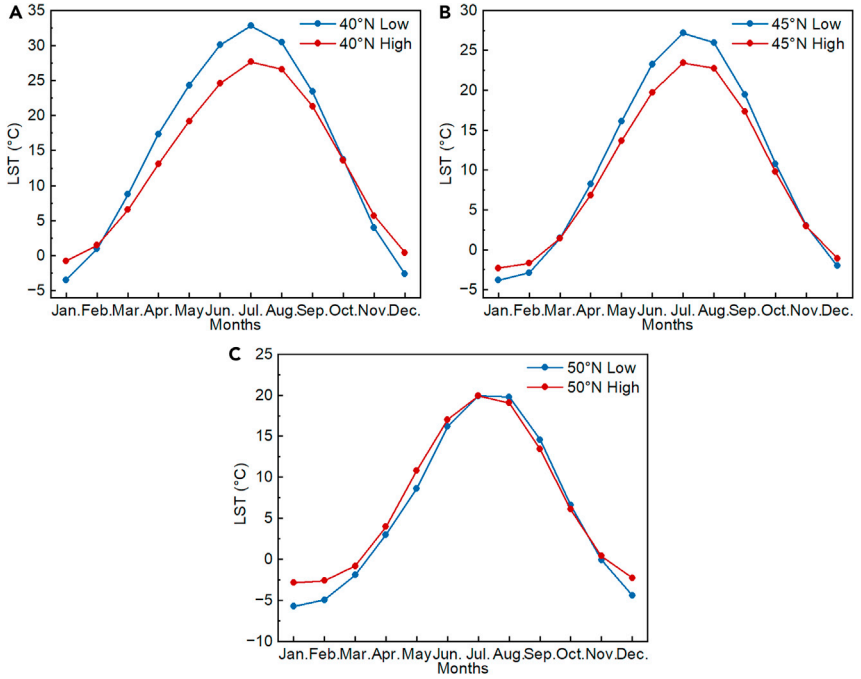


**Figure 3. Intra-annual variation of land surface temperature (LST) in areas of high and low soil moisture at 40°N**

(A) 45°N (B), and 50°N (C). The middle- and high-latitude regions where winter temperatures were below 0° (40°N, 45°N, 50°N, with 5° intervals and a width of 0.5°) were selected, and the LST variation in these regions with two soil moisture backgrounds were extracted: high (>0.4 $m^3/m^3$) and low (<0.2 $m^3/m^3$).

more significant overall intra-annual temperature difference, i.e., the higher temperature in summer and lower temperature in winter. In contrast, the temperature fluctuation was smaller in high-SM areas. Furthermore, this phenomenon was more pronounced in the 40°N and 45°N regions (Figures 3A and 3B). More importantly, the intersection of LST in areas with high and low SM was near 0°C. The positions of the upper and lower distributions of the two lines were replaced when LST was below 0°C, indicating that SM had different effects on LST when LST was above and below 0°C.

To explain the relationship between LST and AH, the variations of multi-year mean downward long-wave radiation with AH were displayed in Figure 4. The downward long-wave radiation displayed an increasing trend with AH at a different latitude. In areas where the SH was less than 4 g/kg, the long-wave radiation was less than 250 $W/m^2$. The areas with high SH were mainly distributed in low latitudes. And in areas where the SH was larger than 16 g/kg, the long-wave radiation was larger than 375 $W/m^2$.

Based on the above analysis, we further analyzed the quantitative relationship between them. Based on Equation 9 in methods, the quantitative relationship between LST and SM, AH was simulated, and a strong relationship was found. The formula was as follows:

$$LST = 0.7210R_n - 2.0357R_nW + 7.6979WQ - 16.1969 \quad R^2 = 0.92 \qquad \text{(Equation 1)}$$

Where $R_n$ is the net radiation, W is the soil moisture, and Q is the atmospheric humidity in the formula. The p values of all three variables were <0.01, indicating that NR, SM, and AH all played an essential role in the interannual variation of LST, and the variation of global LST could be better simulated with these three variables. The sensitivity of LST to SM was −2.0357R + 7.6979Q from the equation, and it can be found that the sensitivity was positive when R < 3.7815 Q, and the LST increased with SM, displaying a warming effect. When R > 3.7815Q, the sensitivity was negative, and LST decreased with SM, displaying a cooling effect.

Furthermore, we calculated the contribution of NR, SM, and AH to the variations of LST in different periods since 2000, with 1981–2000 as the base time (Tab. 1). Overall, the contribution of SM was the largest. The contribution of SM variation to LST exceeded 55% in both the 2001–2010 and 2011–2020

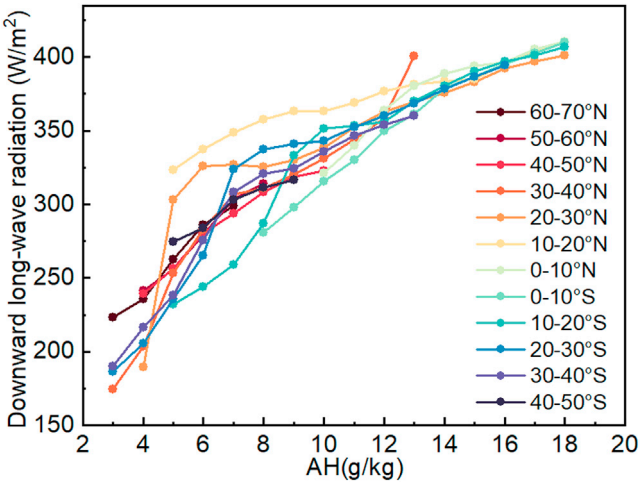


**Figure 4. Variation of downward long-wave radiation with atmospheric humidity (AH) at different latitude**

eras. Moreover, the contribution of NR change was limited, only close to 20%. It was worth noting that the contribution of AH increased from 3.02% in 2001–2010 to 19.91% in 2011–2020. The total contribution of the three factors exceeded 90% in both epochs and 20 years, and the sum of contributions of SM and AH exceeded 72%.

## The heterogeneity of long-term LST change caused by SM and AH

Since the hydrothermal elements varied greatly in different regions of the globe, we again simulated the variation of LST in different regions through NR, SM, and AH. To study the different effects of SM and AH changes on LST, we extracted the trends of SM and AH, respectively. Then four sub-regions were divided according to the different distributions of SM trend and SH trend, including PP region with SM trend >0 and AH trend >0, PN region with SM trend >0 and AH trend <0, NP region with SM trend <0 and AH trend >0, and NN region with SM trend <0 and AH trend <0. The fitting equations of the four sub-regions were displayed in Table 1. The spatial distribution and variables variation of the four sub-regions were displayed in Figure 5. The $R^2$ of the fitted equations exceeded 0.7 in all four sub-regions, especially in the NP and NN regions, where the $R^2$ exceeded 0.93, indicating that NR, SM, and AH can also better portray the variation of LST at the regional scale.

The reasons for LST changes in each sub-region could thus be easily understood from the fitting equations and Figure 5. In the PP region, both SM and SH exhibited a significant upward trend ($p < 0.01$) (Figures 5B and 5C), but the warming and cooling effects of SM changes were different due to the apparent climatic background differences in their distribution. At high latitudes or high-altitude areas, where the annual mean LST was below 0 °C, the increase in SM had a strong warming effect, and the AH also had a warming effect. Hence, the warming trend was evident in northern Asia, the Qinghai-Tibet Plateau, northern Europe, and northern North America (Figure 1B). While in the middle- and low-latitude regions, such as India and Malaysia, the effect of the two was opposite because the mean background temperature was higher than 0°C. So, we fitted the equation for the LST in the PP region where the annual mean LST was higher than 0°C as $LST = 0.7744R_n - 2.7148\ R_nW + 8.5373WQ - 4.5011$. Using 1981–2000 as the background, the LST change due to SM after 2000 was calculated to be - 0.087°C, and the temperature change due to AH was 0.413°C. Therefore, these areas also displayed a warming effect in general. In some parts of India, a cooling trend was also found (Figure 1B) mainly due to the sizable upward trend of SM in this region (>0.05 $m^3/(m^3 \cdot 10a)$ in some areas). The cooling effect caused by SM was above - 3.767°C. In contrast, the warming trend of the significant increase of AH (around 0.3 g/10a) was around 1.236°C, so the LST in this region displayed a decreasing trend.

The PN region was mainly distributed in the northern part of Australia and the southern part of Africa. Since the area was small and mainly close to the ocean, the interannual fluctuations of the elements were significant. The M–K test examined the abrupt change in LST, SM, and AH in the region, and the tipping point

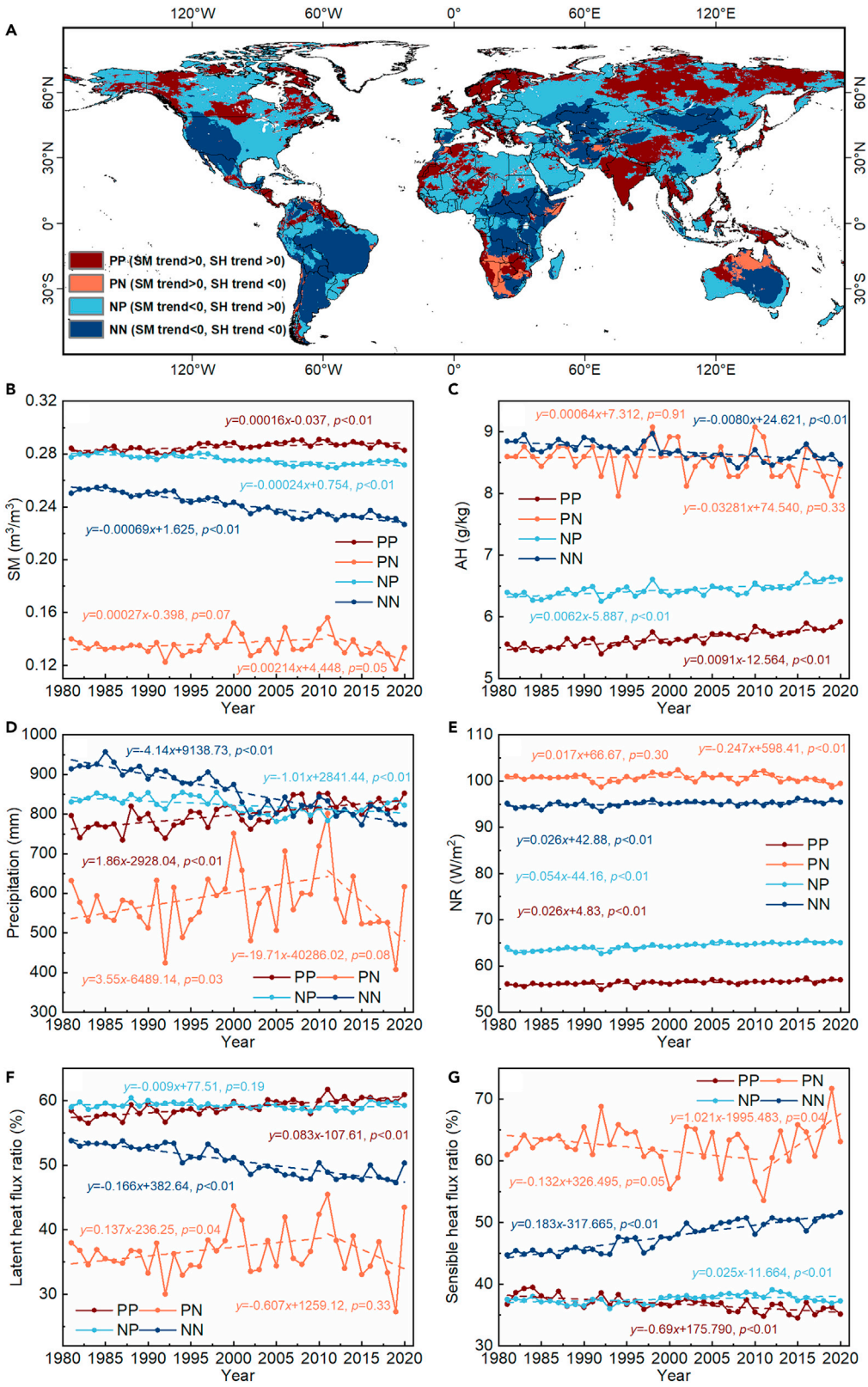
A
120°W
60°W
0°
60°E
120°E
60°N
30°N
0°
30°S
PP (SM trend>0, SH trend >0)
PN (SM trend>0, SH trend <0)
NP (SM trend<0, SH trend >0)
NN (SM trend<0, SH trend <0)
B
SM (m³/m³)
y=0.00016x-0.037, p<0.01
y=-0.00024x+0.754, p<0.01
y=-0.00069x+1.625, p<0.01
y=0.00027x-0.398, p=0.07
y=0.00214x+4.448, p=0.05
PP
PN
NP
NN
Year
C
AH (g/kg)
y=0.00064x+7.312, p=0.91
y=-0.0080x+24.621, p<0.01
y=-0.03281x+74.540, p=0.33
y=0.0062x-5.887, p<0.01
y=0.0091x-12.564, p<0.01
D
Precipitation (mm)
y=-4.14x+9138.73, p<0.01
y=-1.01x+2841.44, p<0.01
y=1.86x-2928.04, p<0.01
y=-19.71x-40286.02, p=0.08
y=3.55x-6489.14, p=0.03
E
NR (W/m²)
y=0.017x+66.67, p=0.30
y=-0.247x+598.41, p<0.01
y=0.026x+42.88, p<0.01
y=0.054x-44.16, p<0.01
y=0.026x+4.83, p<0.01
F
Latent heat flux ratio (%)
y=-0.009x+77.51, p=0.19
y=0.083x-107.61, p<0.01
y=-0.166x+382.64, p<0.01
y=0.137x-236.25, p=0.04
y=-0.607x+1259.12, p=0.33
G
Sensible heat flux ratio (%)
y=1.021x-1995.483, p=0.04
y=-0.132x+326.495, p=0.05
y=0.183x-317.665, p<0.01
y=0.025x-11.664, p<0.01
y=-0.69x+175.790, p<0.01

**Figure 5. Combined effects of soil moisture (SM) and atmospheric moisture (AH) variation on land surface temperature (LST)**

(A) and variations of different zonal elements (B), SM; (C), AH; (D), precipitation; (E), net radiation (NR); (F), latent heat flux ratio; (G), sensible heat flux ratio). In figure a, for areas with SM trend >0 and SH trend >0 (referred to as PP region), areas with SM trend >0 and SH trend <0 (referred to as PN region), areas with SM trend <0 and SH trend >0 (referred to as NP region), and areas with SM trend <0 and SH trend <0 (referred to as NN region).

was around 2011. Therefore, 2011 was selected to separate the whole study period, and the variations of variables were also analyzed in the two periods. During the first 30 years of the study period, the increase in SM caused a significant increase in latent heat flux ratio (Figure 5F) and a significant decrease in sensible heat flux ratio (Figure 5G). Therefore, the LST in this area mainly exhibited a weak decreasing trend (Figure S1). Using 1981–1985 as the background value, the contribution analysis from 1981 to 2010 also displayed the same trend (SM contribution was −0.554°C, AH contribution was 0.011°C). In contrast, during the last ten years of the study period, the trend of all elements changed abruptly, with a significant decrease in SM, leading to a decrease in latent heat flux ratio (Figure 5F) and an increase in sensible heat flux ratio (Figure 5G), which played a significant warming effect. Lower SM reduced evaporation and further reduced latent heat flux ratio and precipitation (Figures 5C and 5D). The greenhouse effect of water vapor also diminished. Therefore, there was a significant temperature increase in this era (Figure S1). The contribution analysis from 2011 to 2020 also displayed the same trend (SM contribution was 1.465°C, AH contribution was −0.195°C).

The areas where SM decreased and AH increased (NP region) were distributed more widely. In the middle and low latitudes, SM and AH showed warming effects, and the LST showed a more apparent increasing trend. In contrast, at high latitudes, there was a cooling effect of decreasing SM, so the magnitude of the cooling effect of SM and the warming effect of atmospheric moisture needs to be weighed in this region. We fitted the equation of LST in the NP region with winter mean LST <0°C as LST = $0.6917R_n$ - $2.2787R_nW$+21.0628WQ - 25.8491 and using 1981–2000 as the background. The variations of LST caused by SM after 2000 were - 0.053°C and 0.815°C caused by AH. Therefore, the LST in this area showed a significant increasing trend.

In the NN area, SM and AH significantly decreased (Figures 5B and 5C). Furthermore, this sub-region was mainly distributed in the middle and low latitudes, so the warming effect of the decreased SM and the cooling effect of the decreased AH were mainly considered. The decrease of SM led to lower evaporation, and smaller latent heat flux ratio (Figure 5F), and a larger sensible heat flux ratio (Figure 5G), which eventually led to a significant increase in LST. Using 1981–2000 as the background, the variation of LST due to SM after 2000 was calculated to be 1.079°C and - 0.373°C caused by AH. Therefore, this region displayed an increasing trend. The warming effect of SM was more significant, and the reduced greenhouse effect of AH did not offset the increase in LST caused by the significant decrease in SM. In addition, this partition contained several regions with significant global LST increases, such as northeastern North America, most of South America, central Africa, western Asia, and central-eastern Asia, where SM decreased significantly.[40–42] The warming effect of SM reduction was much more significant than that of AH change, which was the main reason for the significant warming in these regions.

## DISCUSSION

### Comparison of ERA5-Land dataset

The ERA5-Land analysis data are chosen because of the state-of-art model, good accuracy, and long-time span.[43] According to the previous studies, the accuracy of the ERA5-Land data (soil temperature and soil moisture) can meet the need of this global analysis.[44] Although some other data, such as thermal-based LST data, have high accuracy, it has some drawbacks. For example, thermal-based LST data can only be acquired under cloud-free conditions, and the data acquisition time is specific. Therefore, these data are discontinuous, which can lead to significant biases and cannot support our long-time series study.

We also compare our results with other studies. For LST, it is shown that ERA5-Land data are in good agreement with MODIS, especially in the Arctic region, which shows significant warming.[45] According to the study, the spatial and temporal variability of China merged surface temperature is also in obvious agreement with ERA5-Land data.[46] In addition, two other widely used LST datasets (MODIS and GLDAS) are

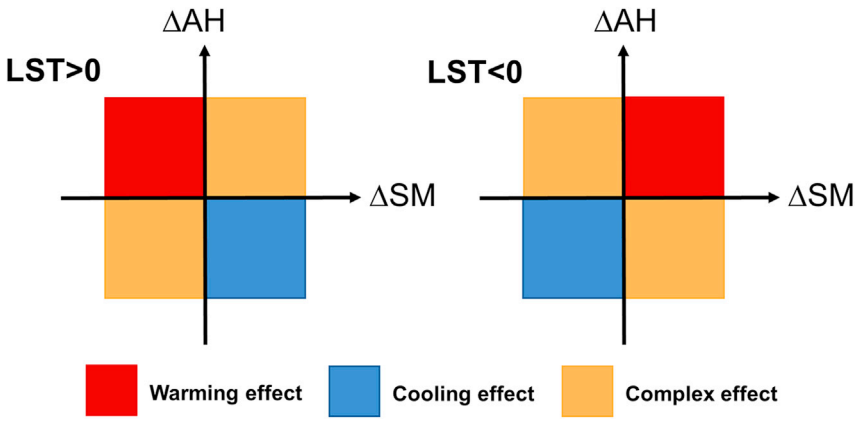


**Figure 6. Patterns of soil moisture (SM) and atmospheric humidity (AH) effects on land surface temperature (LST)**

compared with ERA5-Land data (Figure S1). The global annual mean change trends of the three datasets are consistent. The average difference between ERA5-Land LST and MODIS LST as well as GLDAS LST is 0.09°C. Therefore, we believe that the ERA5-Land LST data can satisfy our study. For soil moisture, the ERA5-Land data showed higher Pearson correlation at 5 cm compared to ERA5 in 64% site with *in situ* measurement from International Soil Moisture Network.[43] In addition, other researchers have analyzed the soil moisture elements of these data from the perspectives of Soil Moisture Active Passive data,[47] model component,[48] and comparison with other gridded data,[49] and concluded that these data have good accuracy. Moreover, it is shown that the long-term daily SM data of ERA-Interim is better at the pixel scale, and the global SM shows a significant decreasing trend from 1979 to 2017,[50] which is consistent with our results. The global AH mainly displays an increasing trend in recent years, mainly because of the global temperature increase. Studies have shown that though the terrestrial specific humidity is increasing, the relative humidity is decreasing.[37] Moreover, there are many overlapping regions where SM and AH significantly decrease (Figures 1D and 1F), among which North America and[41] Central Asia[51,52] have indeed experienced severe droughts in recent years. In contrast, in areas such as central Africa and South America, the decreases in SM and AH may be due to deforestation.[53,54] In addition, the study also showed that 65.1% of the regions with decreasing SM were caused by increasing temperature,[50] which is the main reason why the regions with decreasing SM in the middle and low latitudes overlap with the regions with significant temperature increase. Overall, the ERA5-Land data can better reflect the spatial distribution and temporal trends of the studied variables.

## Interaction mechanisms of SM, AH, and LST

Solar radiation is the dominant factor affecting LST at a certain time, and the amount of NR directly determines the LST. In addition, moisture is the primary regulator of LST, including SM and AH. However, the variation of solar radiation reaching an area was relatively small on an interannual scale, and the variation of moisture was relatively drastic from Table 2. Therefore, moisture variation became the main factor that caused long-term LST variation in an area. However, due to different climatic backgrounds, the role of SM and AH on long-term LST variation showed different degrees of influence. For example, in the high-latitude region, the influence of AH was more extensive (Figure 2B).

In general, the LST mainly exhibits a negative relationship with SM due to the negative feedback between them.[55] However, the relationship between LST and SM is positive in some latitude (especially in high latitude), mainly because of the warming effect of the water freezing.[56] The LST trend with SM above and below 0°C LST background also confirmed our result (Figure S2). In areas with an annual mean LST >0°C, as SM increased, more energy was transported in the form of latent heat flux, and sensible heat flux decreased; therefore, the increase of SM mainly exhibited a cooling effect (Figure S2A).[20,57] In areas where the annual mean LST <0°C, the increase in SM led to more conversion of liquid water to solid water and heat release, which exhibited a warming effect for the land surface, and, conversely, a cooling effect (Figure S2B). Therefore, when discussing the effect of SM, it is necessary to take LST = 0°C as the dividing line and analyze the influencing mechanism at different background temperatures separately.

**Table 1. Fitting equations and the $R^2$ and p value for LST in different sub-regions**

| Sub-regions | Equation | $R^2$ | *P* ($R_n$, W, Q) |
|---|---|---|---|
| PP | LST = 0.4817$R_n$ - 1.6616$R_n$W+13.8307WQ - 20.8246 | 0.84 | <0.01/<0.01/<0.01 |
| PN | LST = 0.0975$R_n$ - 1.0563$R_n$W+4.4251WQ+22.9871 | 0.70 | 0.29/<0.01/0.03 |
| NP | LST = 0.3925$R_n$ - 1.0443$R_n$W+8.5824WQ - 18.1477 | 0.93 | <0.01/<0.01/<0.01 |
| NN | SLT = 0.4877$R_n$ - 1.7439$R_n$W+7.7685WQ - 3.8033 | 0.94 | <0.01/<0.01/<0.01 |

The partial correlation among LST, SM, and AH at annual and seasonal scales also proves our result (Figure S3). On the annual scale, the partial correlation between SM and LST was generally negative, while it was positive for the correlation between AH and LST (FiguresS3A and S3B). In addition, the seasonal correlations between LST and SM were different in different seasons, which means the background temperature background was vital in their relationship. AH and LST displayed a significant positive correlation on the global scale. Therefore, the increase in AH mainly shows a greenhouse effect because the higher AH will increase the downward long-wave radiation and lead to a warmer land surface.[58]

To sum up, SM and AH are essential regulators of LST. SM has opposite effects, i.e., warming and cooling above and below 0°C due to water status transformation. AH mainly exhibits insulation and warming effects. Therefore, when considering the combined effect of SM and AH on LST, it is necessary to classify the background values of LST. We summarized the compound effect pattern of SM and AH on LST in Figure 6. In areas where the mean LST >0, the increase in SM has a cooling effect. While in areas where the mean LST <0, the increase in SM has a warming effect. Then superimposed with the effect of AH, we can obtain the combined effect of SM and AH on LST in different regions.

## The effect of land cover change on the land surface hydrothermal variations in different regions

Land cover change is an important influence factor on land surface hydrothermal conditions. We also analyze the global land cover conversion from 1982 to 2015, select the top 5 conversion types (accounting for 51.8%), and analyze the change of hydrothermal conditions in these areas (Table 3). The distributions of these five land cover conversions are shown in Figure S4. From Table 3, the largest conversion is from grassland to forest ($2.73 \times 10^6$ $km^2$). The areas of grassland converted to forest were mainly distributed in the middle and high latitudes, especially in northern Asia (Figure S4). The conversion of grassland to the forest was mainly due to the rapid warming in this area (Figure 1B), which was favorable to the positive vegetation succession. Areas of forest-to-grassland conversion are concentrated in the central part of South America, a region that has experienced significant forest degradation and agricultural expansion in recent years.[59] The areas where cropland converted to the forest are mainly distributed in southern China and central Europe, where the reduction of cropland and related policies have led to the recovery of the ecosystem.[60,61] In addition, the increasing trend of LST is also the lowest (0.2183°C/10a), and the increasing trend of AH is the most pronounced (0.0409 g/10a) in this area. The conversion of grassland to shrubland is concentrated in eastern South America and southern Africa, where deforestation and agricultural activities have led to the degradation of grassland and significant changes in hydrothermal elements,[35] with the largest downward trends in soil moisture, specific humidity, and precipitation. The areas where grasslands convert to cropland are mainly located in the central part of North America and the southern part of South America, where the expansion of agricultural land led to the degradation and disappearance of grasslands and, therefore, a significant decrease in soil moisture (−0.005 $m^3$/($m^3$·10a)). Overall, it can be seen that the land surface hydrothermal variations result from the combined effect of human activities and climate change. Some previous studies have reached similar conclusions.[62,63]

## Scaling issues for regression analysis

We construct a mechanism-based statistical model according to Equation 9, simplifying the complex coefficient determination process. The equation has a high accuracy and strong explanatory power. Though the global result is good, determining each parameter on a regional scale is very difficult due to the widely varying property of the land surface and the fact that solar radiation is changing at all times. Therefore, detailed regressions are required for the regional analysis. The result of standardized regression

**Table 2. Contributions of net radiation (NR), soil moisture (SM), and atmospheric humidity (AH) to land surface temperature (LST) in different eras**

| | LST variation caused by NR | NR contribution | LST variation caused by SM | SM contribution | LST variation caused by AH | AH contribution | All contribution |
|---|---|---|---|---|---|---|---|
| 2001–2010 | 0.1178 | 21.38% | 0.4050 | 73.52% | 0.0167 | 3.02% | 97.97% |
| 2011–2020 | 0.1552 | 16.45% | 0.5283 | 55.99% | 0.1879 | 19.91% | 92.34% |
| 2001–2020 | 0.1365 | 18.26% | 0.4667 | 62.45% | 0.0766 | 10.25% | 90.96% |

The unit of LST variation is °C.

coefficients also confirmed our thoughts: the importance of SM and AH differed in different regions of the globe, where SM was more important at low and middle latitudes, and AH was more important at higher latitudes arid regions (Figure S4). Therefore, we performed a zonal analysis to interpret the regional LST change.

In addition, the p value of the NR and AH in the PN region was not significant, mainly because of the uncertainty due to the small area. The PN region is mainly distributed in the mid-latitude. The response of LST to atmospheric humidity was relatively small in this latitude, according to the study by Colman et al.[28]

## Conclusions

Based on a novel method combining the scientific principle with statistical analysis, we linked the surface hydrothermal process with climate change, quantitatively revealed the complex relationship between surface water and LST, and disclosed the influencing mechanism of the synergistic change of SM and AH on LST. The results showed that 70.7% of the global land exhibited a significant increase in LST. SM played essential and different roles under the different LST backgrounds. When mean LST was above 0°C, LST decreased with SM, while it increased with SM when mean LST was below 0°C. The AH always displayed a greenhouse effect on the LST. NR, SM, and AH could simulate the LST well and explain 92% of the causes of global LST change. The relationship equation established can explain well the global LST variation in different regions. A framework of the synergistic effect of SM and AH on LST was proposed, which will provide new sight for related research.

The results described previously show that SM and AH have essential effects on climate change, although they change slowly. Intensive human activities have broken the water-energy balance in many regions and led to climate change. Rational regulation of soil hydrothermal processes is the core of sustainable land management. These findings have important implications for understanding the mechanism of global climate change and adapting to it.

## Limitations of the study

Although our study has mechanistically explored the combined effect of SM and AH on LST, some things could be improved regarding data and methods. First, we only use one dataset though it is a state-of-the-art reanalysis dataset.[43] All variables derived from the one system model may have the same error, and its different variables are not independent. Though the results of our analysis suggest that the LST's differences in different datasets are small on a global average, LST might be different at regional scales. Second,

**Table 3. Top five land cover conversion areas and hydrothermal factor change trend from 1982 to 2015**

| Type | Area ($km^2$) | LST trend (°C/10a) | SM trend ($m^3/(m^3 \cdot 10a)$) | AH trend (g/10a) | P trend (mm/10a) |
|---|---|---|---|---|---|
| G-F | $2.73\times10^6$ | 0.3278 | −0.0017 | 0.0368 | −10.17 |
| F-G | $1.80\times10^6$ | 0.3171 | −0.0033 | −0.0112 | −17.45 |
| C-F | $1.79\times10^6$ | 0.2183 | −0.0027 | 0.0409 | −16.71 |
| G-S | $1.78\times10^6$ | 0.2343 | −0.0052 | −0.0911 | −44.79 |
| G-C | $1.63\times10^6$ | 0.3017 | −0.0050 | 0.0127 | −18.81 |

Cropland (C), Forest (F), Grassland (G), Shrubland (S) were the main types in top five conversion. Hydrothermal factor mainly contains Land surface temperature (LST), Soil moisture (SM), Atmospheric humidity (AH), and Precipitation (P).

the conclusions are based on statistical analysis. Different simulations with a global climate model to isolate the impact of certain processes would be better. Third, our study focuses more on the principal explanation of the interannual scale variation of LST other than on seconds, daily, or monthly scale, and an accurate simulation, including capturing human activities (such as irrigation and planting), is also needed in the future work.

## STAR★METHODS

Detailed methods are provided in the online version of this paper and include the following:

- KEY RESOURCES TABLE
- RESOURCE AVAILABILITY
  - Lead contact
  - Materials availability
  - Data and code availability
- METHOD DETAILS
  - Contribution calculation
  - Partial correlation analysis
  - ERA5 and ERA5-Land reanalysis data
  - Land cover data
  - MODIS and GLDAS land surface temperature data

## SUPPLEMENTAL INFORMATION

Supplemental information can be found online at https://doi.org/10.1016/j.isci.2023.106837.

## ACKNOWLEDGMENTS

This paper is supported by the National Key R&D Program of China (No. 2018YFA0606303, No. 2021YFD1901104, and No. 2022YFD1500602).

## AUTHOR CONTRIBUTIONS

Conceptualization, Z.H.P.. and K.J.; Methodology, K.J., X.C., and J.L.W.; Investigation, G.L.H.; Writing – Original Draft, K.J. and Z.H.P.; Writing – Review & Editing, F.F.P., A.J.T., and P.L.A.; Funding Acquisition, Z.H.P.; Supervision, Z.H.P.; Resources, L.C., Z.Y.Z., N.H., S.Q.M., and R.P.G.; Data Curation, Z.Z.Z., J.Y.M., X.Q.L., and Z.Q.D.

## DECLARATION OF INTERESTS

The authors declare no competing interests.

Received: December 14, 2022
Revised: March 1, 2023
Accepted: May 4, 2023
Published: May 9, 2023

## REFERENCES

1. Li, Z.L., Tang, B.H., Wu, H., Ren, H., Yan, G., Wan, Z., Trigo, I.F., and Sobrino, J.A. (2013). Satellite-derived land surface temperature: current status and perspectives. Rem. Sens. Environ. *131*, 14–37. https://doi.org/10.1016/j.rse.2012.12.008.

2. IPCC (2021). limate Change 2021: The Physical Science Basis. Contribution of Working Group I to the Sixth Assessment Report of the Intergovernmental Panel on Climate Change. Cambridge University Press. https://doi.org/10.1017/9781009157896.

3. Andrade, M., De Marchi, L., Soares, A., Rocha, R.J.M., Figueira, E., and Freitas, R. (2019). Are the effects induced by increased temperature enhanced in Mytilus galloprovincialis submitted to air exposure? Sci. Total Environ. *647*, 431–440. https://doi.org/10.1016/j.scitotenv.2018.07.293.

4. Kong, H., Wang, Z., Guo, J.Y., Xia, Q.Y., Zhao, H., Zhang, Y.L., Guo, A.P., and Lu, B.R. (2021). Increases in genetic diversity of weedy rice associated with ambient temperatures and limited gene flow. Biology *10*, 71. https://doi.org/10.3390/biology10020071.

5. Li, S., and Xiao, B. (2022). Cyanobacteria and moss biocrusts increase evaporation by regulating surface soil moisture and temperature on the northern Loess Plateau, China. Catena *212*, 106068. https://doi.org/10.1016/j.catena.2022.106068.

6. Berg, A., Findell, K., Lintner, B., Giannini, A., Seneviratne, S.I., van den Hurk, B., Lorenz, R., Pitman, A., Hagemann, S., Meier, A., et al. (2016). Land-atmosphere feedbacks amplify aridity increase over land under global warming. Nat. Clim. Change *6*, 869–874. https://doi.org/10.1038/nclimate3029.

7. Lal, P., Dubey, A.K., Kumar, A., Kumar, P., and Dwivedi, C.S. (2022). Measuring the control of landscape modifications on surface temperature in India. Geocarto Int. *37*, 15736–15753. https://doi.org/10.1080/10106049.2022.2102224.

8. Yang, J., Ren, J., Sun, D., Xiao, X., Xia, J.C., Jin, C., and Li, X. (2021). Understanding land surface temperature impact factors based on local climate zones. Sustain. Cities Soc. *69*, 102818. https://doi.org/10.1016/j.scs.2021.102818.

9. Mushore, T.D., Mutanga, O., Odindi, J., and Dube, T. (2017). Linking major shifts in land surface temperatures to long term land use and land cover changes: a case of Harare, Zimbabwe. Urban Clim. *20*, 120–134. https://doi.org/10.1016/j.uclim.2017.04.005.

10. Wongsai, N., Wongsai, S., Lim, A., McNeil, D., and Huete, A.R. (2020). Impacts of spatial heterogeneity patterns on long-term trends of Moderate Resolution Imaging Spectroradiometer (MODIS) land surface temperature time series. J. Appl. Remote Sens. *14*, 1. https://doi.org/10.1117/1.Jrs.14.014513.

11. NourEldeen, N., Mao, K., Yuan, Z., Shen, X., Xu, T., and Qin, Z. (2020). Analysis of the spatiotemporal change in land surface temperature for a long-term sequence in Africa (2003-2017). Rem. Sens. *12*, 488. https://doi.org/10.3390/rs12030488.

12. Naga Rajesh, A., Abinaya, S., Purna Durga, G., and Lakshmi Kumar, T.V. (2023). Long-term relationships of MODIS NDVI with rainfall, land surface temperature, surface soil moisture and groundwater storage over monsoon core region of India. Arid Land Res. Manag. *37*, 51–70. https://doi.org/10.1080/15324982.2022.2106323.

13. Tayyebi, A., Shafizadeh-Moghadam, H., and Tayyebi, A.H. (2018). Analyzing long-term spatio-temporal patterns of land surface temperature in response to rapid urbanization in the mega-city of Tehran. Land Use Pol. *71*, 459–469. https://doi.org/10.1016/j.landusepol.2017.11.023.

14. Gevaert, A.I., Miralles, D.G., de Jeu, R.A.M., Schellekens, J., and Dolman, A.J. (2018). Soil moisture-temperature coupling in a set of land surface models. J. Geophys. Res. Atmos. *123*, 1481–1498. https://doi.org/10.1002/2017jd027346.

15. Dessler, A.E., Zhang, Z., and Yang, P. (2008). Water-vapor climate feedback inferred from climate fluctuations. Geophys. Res. Lett. *35*, L20704–L22008. https://doi.org/10.1029/2008GL035333.

16. Liu, J., Hagan, D.F.T., and Liu, Y. (2021). Global land surface temperature change (2003-2017) and its relationship with climate drivers: AIRS, MODIS, and ERA5-land based analysis. Rem. Sens. *13*, 44. https://doi.org/10.3390/rs13010044.

17. Gleeson, T., Wang-Erlandsson, L., Porkka, M., Zipper, S.C., Jaramillo, F., Gerten, D., Fetzer, I., Cornell, S.E., Piemontese, L., Gordon, L.J., et al. (2020). Illuminating water cycle modifications and Earth system resilience in the Anthropocene. Water Resour. Res. *56*. https://doi.org/10.1029/2019wr024957.

18. Shi, H., Jin, F.F., Wills, R.C.J., Jacox, M.G., Amaya, D.J., Black, B.A., Rykaczewski, R.R., Bograd, S.J., García-Reyes, M., and Sydeman, W.J. (2022). Global decline in ocean memory over the 21st century. Sci. Adv. *8*, eabm3468. https://doi.org/10.1126/sciadv.abm3468.

19. Sohail, T., Zika, J.D., Irving, D.B., and Church, J.A. (2022). Observed poleward freshwater transport since 1970. Nature *602*, 617–622. https://doi.org/10.1038/s41586-021-04370-w.

20. Talib, J., Taylor, C.M., Duan, A., and Turner, A.G. (2021). Intraseasonal soil moisture-atmosphere feedbacks on the Tibetan plateau circulation. J. Clim. *34*, 1789–1807. https://doi.org/10.1175/jcli-d-20-0377.1.

21. Hauser, M., Orth, R., and Seneviratne, S.I. (2016). Role of soil moisture versus recent climate change for the 2010 heat wave in western Russia. Geophys. Res. Lett. *43*, 2819–2826. https://doi.org/10.1002/2016gl068036.

22. Miralles, D.G., Teuling, A.J., van Heerwaarden, C.C., and Vilà-Guerau de Arellano, J. (2014). Mega-heatwave temperatures due to combined soil desiccation and atmospheric heat accumulation. Nat. Geosci. *7*, 345–349. https://doi.org/10.1038/Ngeo2141.

23. Fischer, E.M., Seneviratne, S.I., Vidale, P.L., Lüthi, D., and Schär, C. (2007). Soil moisture - atmosphere interactions during the 2003 European summer heat wave. J. Clim. *20*, 5081–5099. https://doi.org/10.1175/Jcli4288.1.

24. AghaKouchak, A., Farahmand, A., Melton, F.S., Teixeira, J., Anderson, M.C., Wardlow, B.D., and Hain, C.R. (2015). Remote sensing of drought: progress, challenges and opportunities. Rev. Geophys. *53*, 452–480. https://doi.org/10.1002/2014rg000456.

25. Berg, A., and Sheffield, J. (2018). Climate change and drought: the soil moisture perspective. Curr. Clim. Change Rep. *4*, 180–191. https://doi.org/10.1007/s40641-018-0095-0.

26. Seneviratne, S.I., Corti, T., Davin, E.L., Hirschi, M., Jaeger, E.B., Lehner, I., Orlowsky, B., and Teuling, A.J. (2010). Investigating soil moisture-climate interactions in a changing climate: a review. Earth Sci. Rev. *99*, 125–161. https://doi.org/10.1016/j.earscirev.2010.02.004.

27. Vihma, T., Screen, J., Tjernström, M., Newton, B., Zhang, X., Popova, V., Deser, C., Holland, M., and Prowse, T. (2016). The atmospheric role in the Arctic water cycle: a review on processes, past and future changes, and their impacts. J. Geophys. Res. Biogeosci. *121*, 586–620. https://doi.org/10.1002/2015jg003132.

28. Colman, R.A., and Hanson, L.I. (2013). On atmospheric radiative feedbacks associated with climate variability and change. Clim. Dynam. *40*, 475–492. https://doi.org/10.1007/s00382-012-1391-3.

29. Feng, H., and Zou, B. (2019). A greening world enhances the surface-air temperature difference. Sci. Total Environ. *658*, 385–394. https://doi.org/10.1016/j.scitotenv.2018.12.210.

30. Bierkens, M.F.P., and Wada, Y. (2019). Non-renewable groundwater use and groundwater depletion: a review. Environ. Res. Lett. *14*, 063002. https://doi.org/10.1088/1748-9326/ab1a5f.

31. Devineni, N., Perveen, S., and Lall, U. (2022). Solving groundwater depletion in India while achieving food security. Nat. Commun. *13*, 3374. https://doi.org/10.1038/s41467-022-31122-9.

32. Lutz, A.F., Immerzeel, W.W., Siderius, C., Wijngaard, R.R., Nepal, S., Shrestha, A.B., Wester, P., and Biemans, H. (2022). South Asian agriculture increasingly dependent on meltwater and groundwater. Nat. Clim. Change *12*, 566–573. https://doi.org/10.1038/s41558-022-01355-z.

33. Wu, R., Li, Z., and Wang, S. (2021). The varying driving forces of urban land expansion in China: insights from a spatial-temporal analysis. Sci. Total Environ. *766*, 142591. https://doi.org/10.1016/j.scitotenv.2020.142591.

34. Boulton, C.A., Lenton, T.M., and Boers, N. (2022). Pronounced loss of Amazon rainforest resilience since the early 2000s. Nat. Clim. Change *12*, 271–278. https://doi.org/10.1038/s41558-022-01287-8.

35. Bardgett, R.D., Bullock, J.M., Lavorel, S., Manning, P., Schaffner, U., Ostle, N., Chomel, M., Durigan, G., L Fry, E., Johnson, D., et al. (2021). Combatting global grassland degradation. Nat. Rev. Earth Environ. *2*, 720–735. https://doi.org/10.1038/s43017-021-00207-2.

36. Lal, P., Shekhar, A., Gharun, M., and Das, N.N. (2023). Spatiotemporal evolution of global long-term patterns of soil moisture. Sci. Total Environ. *867*, 161470. https://doi.org/10.1016/j.scitotenv.2023.161470.

37. Byrne, M.P., and O'Gorman, P.A. (2018). Trends in continental temperature and humidity directly linked to ocean warming. Proc. Natl. Acad. Sci. USA *115*, 4863–4868. https://doi.org/10.1073/pnas.1722312115.

38. Dorigo, W.A., Gruber, A., De Jeu, R.A.M., Wagner, W., Stacke, T., Loew, A., Albergel, C., Brocca, L., Chung, D., Parinussa, R.M., and Kidd, R. (2015). Evaluation of the ESA CCI soil moisture product using ground-based observations. Rem. Sens. Environ. *162*, 380–395. https://doi.org/10.1016/j.rse.2014.07.023.

39. Hersbach, H., Bell, B., Berrisford, P., Hirahara, S., Horányi, A., Muñoz-Sabater, J., Nicolas, J., Peubey, C., Radu, R., Schepers, D., et al. (2020). The ERA5 global reanalysis. Q. J. R.

Meteorol. Soc. *146*, 1999–2049. https://doi.org/10.1002/qj.3803.

40. Tao, F., Yokozawa, M., Hayashi, Y., and Lin, E. (2003). Changes in agricultural water demands and soil moisture in China over the last half-century and their effects on agricultural production. Agric. For. Meteorol. *118*, 251–261. https://doi.org/10.1016/S0168-1923(03)00107-2.

41. Herrera-Estrada, J.E., Martinez, J.A., Dominguez, F., Findell, K.L., Wood, E.F., and Sheffield, J. (2019). Reduced moisture transport linked to drought propagation across north America. Geophys. Res. Lett. *46*, 5243–5253. https://doi.org/10.1029/2019gl082475.

42. Liu, Y., Liu, Y., Wang, W., Fan, X., and Cui, W. (2022). Soil moisture droughts in East Africa: spatiotemporal patterns and climate drivers. J Hydrol-Reg Stud *40*, 101013.

43. Muñoz-Sabater, J., Dutra, E., Agustí-Panareda, A., Albergel, C., Arduini, G., Balsamo, G., Boussetta, S., Choulga, M., Harrigan, S., Hersbach, H., et al. (2021). ERA5-Land: a state-of-the-art global reanalysis dataset for land applications. Earth Syst. Sci. Data *13*, 4349–4383. https://doi.org/10.5194/essd-13-4349-2021.

44. Li, M., Wu, P., and Ma, Z. (2020). A comprehensive evaluation of soil moisture and soil temperature from third-generation atmospheric and land reanalysis data sets. Int. J. Climatol. *40*, 5744–5766. https://doi.org/10.1002/joc.6549.

45. Wang, Y.R., Hessen, D.O., Samset, B.H., and Stordal, F. (2022). Evaluating global and regional land warming trends in the past decades with both MODIS and ERA5-Land land surface temperature data. Rem. Sens. Environ. *280*, 113181. https://doi.org/10.1016/j.rse.2022.113181.

46. Li, Q., Sun, W., Yun, X., Huang, B., Dong, W., Wang, X.L., Zhai, P., and Jones, P. (2021). An updated evaluation of the global mean land surface air temperature and surface temperature trends based on CLSAT and CMST. Clim. Dynam. *56*, 635–650. https://doi.org/10.1007/s00382-020-05502-0.

47. Lal, P., Singh, G., Das, N.N., Colliander, A., Entekhabi, D., and Coccetti, A. (2022). Assessment of ERA5-land volumetric soil water layer product using in situ and SMAP soil moisture observations. Ieee Geosci Remote S *19*, 1–5. https://doi.org/10.1109/LGRS.2022.3223985.

48. Wu, Z., Feng, H., He, H., Zhou, J., and Zhang, Y. (2021). Evaluation of soil moisture climatology and anomaly components derived from ERA5-land and GLDAS-2.1 in China. Water Resour. Manag. *35*, 629–643. https://doi.org/10.1007/s11269-020-02743-w.

49. Xing, Z., Fan, L., Zhao, L., De Lannoy, G., Frappart, F., Peng, J., Li, X., Zeng, J., Al-Yaari, A., Yang, K., et al. (2021). A first assessment of satellite and reanalysis estimates of surface and root-zone soil moisture over the permafrost region of Qinghai-Tibet Plateau. Rem. Sens. Environ. *265*, 112666. https://doi.org/10.1016/j.rse.2021.112666.

50. Deng, Y., Wang, S., Bai, X., Luo, G., Wu, L., Cao, Y., Li, H., Li, C., Yang, Y., Hu, Z., and Tian, S. (2020). Variation trend of global soil moisture and its cause analysis. Ecol. Indicat. *110*, 105939. https://doi.org/10.1016/j.ecolind.2019.105939.

51. Yuan, Y., Bao, A., Jiang, P., Hamdi, R., Termonia, P., De Maeyer, P., Guo, H., Zheng, G., Yu, T., and Prishchepov, A.V. (2022). Probabilistic assessment of vegetation vulnerability to drought stress in Central Asia. J. Environ. Manag. *310*, 114504.

52. Deng, H., Yin, Y., and Han, X. (2020). Vulnerability of vegetation activities to drought in Central Asia. Environ. Res. Lett. *15*, 084005. https://doi.org/10.1088/1748-9326/ab93fa.

53. Salazar, A., Katzfey, J., Thatcher, M., Syktus, J., Wong, K., and McAlpine, C. (2016). Deforestation changes land-atmosphere interactions across South American biomes. Global Planet. Change *139*, 97–108. https://doi.org/10.1016/j.gloplacha.2016.01.004.

54. Duku, C., and Hein, L. (2021). The impact of deforestation on rainfall in Africa: a data-driven assessment. Environ. Res. Lett. *16*, 064044. https://doi.org/10.1088/1748-9326/abfcfb.

55. Cheruy, F., Dufresne, J.L., Aït Mesbah, S., Grandpeix, J.Y., and Wang, F. (2017). Role of soil thermal inertia in surface temperature and soil moisture-temperature feedback. J. Adv. Model. Earth Syst. *9*, 2906–2919. https://doi.org/10.1002/2017ms001036.

56. Hu, H., Ye, B., Zhou, Y., and Tian, F. (2006). A land surface model incorporated with soil freeze/thaw and its application in GAME/Tibet. Sci. China Earth Sci. *49*, 1311–1322. https://doi.org/10.1007/s11430-006-2028-3.

57. Wouters, H., Keune, J., Petrova, I.Y., van Heerwaarden, C.C., Teuling, A.J., Pal, J.S., Vilà-Guerau de Arellano, J., and Miralles, D.G. (2022). Soil drought can mitigate deadly heat stress thanks to a reduction of air humidity. Sci. Adv. *8*, eabe6653. https://doi.org/10.1126/sciadv.abe6653.

58. Vargas Zeppetello, L.R., Donohoe, A., and Battisti, D.S. (2019). Does surface temperature respond to or determine downwelling longwave radiation? Geophys. Res. Lett. *46*, 2781–2789. https://doi.org/10.1029/2019gl082220.

59. Paredes-Trejo, F., Barbosa, H., Giovannettone, J., Kumar, T.V.L., Kumar Thakur, M., and de Oliveira Buriti, C. (2022). Drought variability and land degradation in the Amazon River basin. Front. Earth Sci. *10*, 939908. https://doi.org/10.3389/feart.2022.939908.

60. Liu, P., Liu, X., Dai, Y., Feng, Y., Zhang, Q., and Chu, G. (2020). Influence of vegetation restoration on soil hydraulic properties in south China. Forests *11*, 1111. https://doi.org/10.3390/f11101111.

61. Zerbe, S. (2002). Restoration of natural broad-leaved woodland in Central Europe on sites with coniferous forest plantations. For. Ecol. Manag. *167*, 27–42. https://doi.org/10.1016/s0378-1127(01)00686-7.

62. Zhang, J., Yang, J., An, P., Ren, W., Pan, Z., Dong, Z., Han, G., Pan, Y., Pan, S., and Tian, H. (2017). Enhancing soil drought induced by climate change and agricultural practices: observational and experimental evidence from the semiarid area of northern China. Agric. For. Meteorol. *243*, 74–83. https://doi.org/10.1016/j.agrformet.2017.05.008.

63. Liu, Y., Pan, Z., Zhuang, Q., Miralles, D.G., Teuling, A.J., Zhang, T., An, P., Dong, Z., Zhang, J., He, D., et al. (2015). Agriculture intensifies soil moisture decline in Northern China. Sci. Rep. *5*, 11261. https://doi.org/10.1038/srep11261.

64. Beer, C., Reichstein, M., Tomelleri, E., Ciais, P., Jung, M., Carvalhais, N., Rödenbeck, C., Arain, M.A., Baldocchi, D., Bonan, G.B., et al. (2010). Terrestrial gross carbon dioxide uptake: global distribution and covariation with climate. Science *329*, 834–838. https://doi.org/10.1126/science.1184984.

65. Jiang, K., Pan, Z., Pan, F., Wang, J., Han, G., Song, Y., Zhang, Z., Huang, N., Ma, S., and Chen, X. (2022). Influence patterns of soil moisture change on surface-air temperature difference under different climatic background. Sci. Total Environ. *822*, 153607. https://doi.org/10.1016/j.scitotenv.2022.153607.

66. Longo-Minnolo, G., Vanella, D., Consoli, S., Pappalardo, S., and Ramírez-Cuesta, J.M. (2022). Assessing the use of ERA5-Land reanalysis and spatial interpolation methods for retrieving precipitation estimates at basin scale. Atmos. Res. *271*, 106131. https://doi.org/10.1016/j.atmosres.2022.106131.

67. Barbosa, S., and Scotto, M.G. (2022). Extreme heat events in the Iberia Peninsula from extreme value mixture modeling of ERA5-Land air temperature. Weather Clim. Extrem. *36*, 100448. https://doi.org/10.1016/j.wace.2022.100448.

68. Liu, H., Gong, P., Wang, J., Clinton, N., Bai, Y., and Liang, S. (2020). Annual dynamics of global land cover and its long-term changes from 1982 to 2015. Earth Syst. Sci. Data *12*, 1217–1243. https://doi.org/10.5194/essd-12-1217-2020.

## STAR★METHODS

### KEY RESOURCES TABLE

| REAGENT or RESOURCE | SOURCE | IDENTIFIER |
|---|---|---|
| Deposited data | | |
| Land surface component dataset | ECMWF | https://cds.climate.copernicus.eu/ |
| Land cover data | GLASS-GLC | https://doi.pangaea.de/10.1594/PANGAEA.913496 |
| MODIS LST data | NASA | https://search.earthdata.nasa.gov/search |
| GLDAS LST data | NASA | https://disc.gsfc.nasa.gov/datasets |
| Software and algorithms | | |
| ArcGIS | Esri | ArcGIS 10.2 |
| ENVI | Exelis Visual Information Solutions | ENVI 5.3 |
| MATLAB | MathWorks | MATLAB R2016a |
| Origin | OriginLab | Origin 2022 |

### RESOURCE AVAILABILITY

#### Lead contact

Further information and requests for data should be directed to and will be fulfilled by the lead contact, Zhihua Pan (panzhihua@cau.edu.cn).''

#### Materials availability

This study did not generate new unique materials.

#### Data and code availability

The datasets and code supporting the current study have not been deposited in a public repository but are available from the lead contact on request.

### METHOD DETAILS

The equation of the relationship between surface temperature and net radiation, soil moisture, and atmospheric humidity.

According to the connotation of heat capacity, the energy required to heat soil of a specific volume ($V$, $m^3$), when its temperature changes from the initial $T_1$ (°C) to the end $T_2$ (°C) in a specific time $dt$ (day, month or year) is:

$$\frac{dQ}{dt} = \frac{C_v V d(T_2 - T_1)}{dt} = \frac{C_v V dT}{dt} \quad \text{(Equation 2)}$$

Where $C_V$ is the soil heat capacity (J/(°C·$m^3$)). If the energy comes from solar radiation, it is equivalent to the soil heat flux, and it can be obtained from the land surface energy balance equation:

$$\frac{dQ}{dt} = R_n - \lambda E - SH \quad \text{(Equation 3)}$$

Where $dQ/dt$ represents the energy change ($dQ$) in a given volume of soil and during a unit time ($dt$), $R_n$ is net radiation (J/($m^2$·d)) at the land surface, $\lambda E$ is latent heat flux (J/($m^2$·d)), $SH$ denotes sensible heat flux (J/($m^2$·d)).

From the Equations 1 and 2, it can be written as:

$$\frac{dT}{dt} = \frac{(R_n - \lambda E - SH)}{C_v V} = \frac{[(R_n - (\lambda E + SH)]}{C_v V} \quad \text{(Equation 4)}$$

The Bowen's ratio is $\beta = H/\lambda E$, so the Equation 4 can be written as:

$$\frac{dT}{dt} = \frac{(R_n - (1+\beta)\lambda E)}{C_v V} \quad \text{(Equation 5)}$$

Theoretically speaking, $(\lambda E / R_n)$ is the function of soil moisture (W) without considering atmospheric humidity effects,[26] which is:

$$\lambda E / R_n = f(W) \quad \text{(Equation 6)}$$

In fact, the soil interacts with the atmosphere. Soil evapotranspiration is also affected by atmospheric water vapor. Atmospheric water vapor has large heat storage due to its high heat capacity. It acts like an insulating layer covering the land surface, absorbing and preventing the heat from the ground radiating to the sky. Therefore, both net radiation and atmospheric humidity should be considered when calculating the land surface latent heat flux, and the influence of atmospheric humidity should be considered when calculating the actual LST change in the land-atmosphere system, as follows:

$$\lambda E / (R_n - hQ) = f(W) \quad \text{(Equation 7)}$$

Where h is atmospheric water vapor enthalpy (J/g), and Q is the atmospheric humidity (g/kg). We can get the equation from Equations 5 and 7:

$$\frac{dT}{dt} = \frac{(R_n - f(W)(1+\beta)((R_n - hQ))}{C_v V} = \frac{(R_n - f(W)(1+\beta)R_n + f(W)(1+\beta)hQ)}{C_v V} \quad \text{(Equation 8)}$$

This can be simplified as:

$$\frac{dT}{dt} = aR_n - bf(W)R_n + cf(W)Q \quad \text{(Equation 9)}$$

Where, $a = 1/(C_V V)$, $b=(1+\beta)/(C_V V)$, $c=(1+\beta)h/(C_V V)$. These coefficients are determined by specific geographical conditions and temperature background. These coefficients can be obtained by multi-linear regression if long time series of T, $R_n$, W, and Q data are available.

## Contribution calculation

In order to calculate the contribution of net radiation, soil moisture, and atmospheric humidity to the LST change, we take the partial derivative of each of the three elements according to the regression equation obtained and then calculate the contribution of different elements to the LST change from 2001 to 2010 and from 2011 to 2020, using 1981–2000 as the background value. The formula is as follows:

$$Contribution = \frac{\frac{\partial LST}{\partial S} \times \Delta S}{\Delta LST} \times 100\% \quad \text{(Equation 10)}$$

## Partial correlation analysis

In order to analyze the correlation between Ts and soil moisture and specific humidity, partial correlation analysis[64] was conducted on LST, SM, and SH yearly data, and a correlation coefficient was used to express the correlation intensity between LST, SM, and AH.

## ERA5 and ERA5-Land reanalysis data

ERA5 is a new generation of reanalysis data released by the European Center for Medium-Range Weather Forecasts (ECMWF), which has been significantly improved in accuracy due to the development of model physics.[39] ERA5-Land is an enhanced ERA5 surface component dataset that describes surface hydrothermal variability and has a globally improved spatial resolution of 9 km (0.1°) created by a more advanced surface modeling technique and has been widely used for regional and global analysis.[16,45,65–67]

The main parameters in this paper were also extracted from the ERA5-Land dataset, including land surface temperature (LST), surface soil moisture (0–7 cm), snow cover percentage, surface net solar radiation, and surface net thermal radiation. The net radiation (NR) used in this study is the subtraction of surface net solar radiation and surface net thermal radiation. The specific humidity at 1000 hPa was chosen to represent the atmospheric humidity and downloaded from ERA5 reanalysis data with a spatial resolution of 0.25°. And the unit of specific humidity is g/kg. The monthly data for these variables for 1981–2020 were utilized in

this study. For the analysis of atmospheric humidity and other factors, such as LST, the ERA5-Land LST data were resampled to 0.25° to be consistent with the atmospheric data.

### Land cover data

The GLASS-GLC (The Global Land Surface Satellite-Global Land Cover) data set is the first record of 34-year long annual dynamics of global land cover spanning from 1982 to 2015 at 5 km resolution. This data integrated the latest version of GLASS CDRs (Climate Data Records) and generated on the Google Earth Engine (GEE) platform. The data contains 7 land cover types, including cropland, forest, grassland, shrubland, tundra, barren land, and snow/ice and the average overall accuracy for the 34 years data is 82.81%.[68] The 1982 and 2015 land cover map were selected, and land cover conversion analysis was done in ArcGIS software.

### MODIS and GLDAS land surface temperature data

Moderate-resolution Imaging Spectroradiometer (MODIS) LST data and Global Land Data Assimilation System (GLDAS) 2.0 reanalysis data are the two most used LST data. They are both from National Aeronautics and Space Administration (NASA) and can be download from https://search.earthdata.nasa.gov/search and https://disc.gsfc.nasa.gov/datasetsrespectively. The MODIS product MOD11C3 was downloaded, which is a global 0.05° LST monthly maximum data for the period 2001–2020. GLDAS 2.0 LST is a global 0.25° LST monthly data for the period 1981–2014. The data are synthesized into annual mean data by ENVI software.